SAND2013-10649C

Toward Transition Statistics Measured on a 7-Degree Hypersonic Cone for Turbulent Spot Modeling

Katya M. Casper*, Steven J. Beresh†, John F. Henfling‡, and Russell W. Spillers§
Sandia National Laboratories, Albuquerque, NM 87185

High-frequency pressure sensors were used in conjunction with a high-speed schlieren system to study the growth and breakdown of boundary-layer disturbances into turbulent spots on a 7° cone in the Sandia Hypersonic Wind Tunnel at Mach 5 and 8. In order to relate the intermittent disturbances to the average characteristics of transition on the cone, the statistical distribution of these disturbances must be known. These include the boundary-layer intermittency, burst rate, and the distribution of disturbance lengths.

Traditional low-speed methods to characterize intermittency identify only turbulent/non-turbulent regions. However at high M, instability waves become an important part of the transitional region. Algorithms to distinguish instability waves from turbulence in both the pressure and schlieren measurements have been developed and the corresponding intermittency of both regions has been computed over a range of Re and M. Separating instability waves from turbulence gives a better description of the intermittent boundary layer at high M and will allow the fluctuations associated with boundary-layer instabilities to be incorporated into transitional models.

Nomenclature

δ	boundary-layer thickness (mm)	Re	freestream unit Reynolds number (1/m)
f	camera framing rate and frequency (kHz)	t	time (s)
M	freestream Mach number	T_0	tunnel stagnation temperature (K)
P_0	tunnel stagnation pressure (kPa)	x	axial model coordinate measured from nose (m)
p'	pressure fluctuation, $p - p_e$ (Pa)		
p_e	boundary-layer edge pressure (Pa)		

I. Introduction

Hypersonic reentry vehicles are subjected to high levels of fluctuating pressures. These intense fluctuations can cause vibration of internal components and lead to structural problems. There is a need to predict the magnitude, frequency content, location, and spatial extent of the pressure fluctuations to better design hypersonic flight vehicles. Current designs often use overly conservative estimates of the fluctuations which lead to heavier vehicles and degraded flight performance. Some correlations exist for the magnitude of transitional and turbulent pressure fluctuations, but these were derived primarily using either incompressible data or conventional (noisy flow) hypersonic wind-tunnel tests.[1] Such modeling efforts have not led to sufficient physical understanding of the transitional pressure fluctuations or to adequate predictive capabilities. Modern computational capabilities seem likely to enable higher-fidelity models in the future if they have a better scientific basis on which to build.

*Senior Member of the Technical Staff, Engineering Sciences Center, Member AIAA, kmcaspe@sandia.gov, (505) 844-1574
†Principal Member of the Technical Staff, Engineering Sciences Center, Associate Fellow AIAA
‡Distinguished Technologist, Member AIAA
§Principal Technologist

Sandia National Laboratories is a multi-program laboratory managed and operated by Sandia Corporation, a wholly owned subsidiary of Lockheed Martin Corporation, for the U.S. Department of Energy's National Nuclear Security Administration under contract DE-AC04-94AL85000.

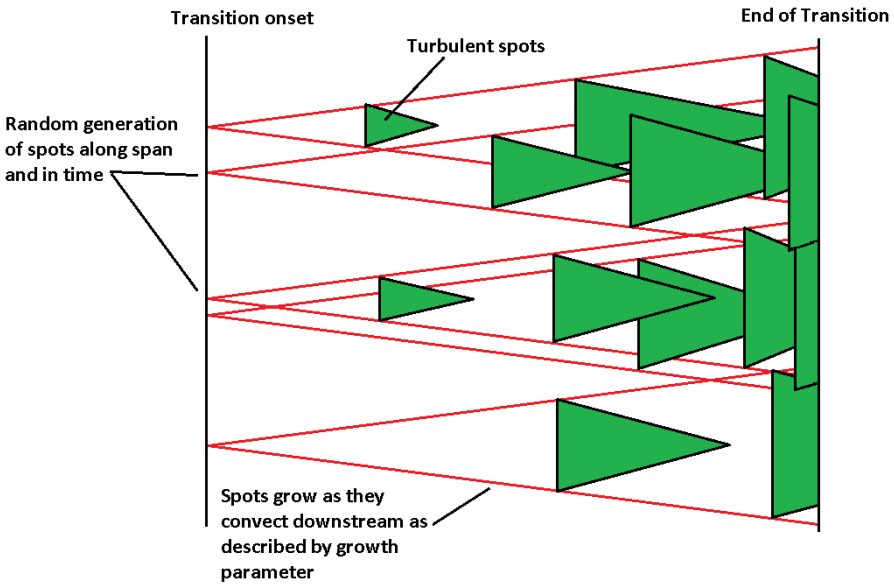

Figure 1. Schematic of turbulent-spot model of transition.

During boundary-layer transition, the heating rates and pressure fluctuations that are experienced are higher than for a fully turbulent boundary layer.[2–6] These high pressure fluctuations result from repeated intermittent spatial-temporal switching between laminar and turbulent regions, creating a broad spectrum of disturbances. Unfortunately in flight, natural transition typically occurs over a large portion of the vehicle,[7] making transitional fluctuations of primary interest for this work.

The transition process can be described through intermittency and the growth and propagation of turbulent spots in the transitional boundary layer.[8,9] Fig. 1 shows a schematic of this model, though with far fewer turbulent spots than a real transition scenario. The model assumes concentrated breakdown in which the turbulent spots are generated near a single streamwise location. The spots are randomly generated along the span and in time. Upstream and downstream of transition onset, no new spots are generated. A spot growth parameter describes the lateral and streamwise growth of the spots as they convect downstream. There are three main parameters that completely describe this model of transition: the transition onset location, the spot formation rate per unit span, and a spot growth parameter. Knowing these values, the transition length can be computed.

This type of transition model allows the computation of flow properties throughout transition.[10–12] For example, by combining the pressure fluctuations associated with wave packets and turbulent spots with this model of transition, the models can be extended to calculate transitional pressure fluctuations from fundamental physics. This type of model has already been developed for incompressible flow on a flat plate.[12]

In order to develop similar models at high speeds and to improve prediction of hypersonic pressure fluctuations, experiments were conducted on a 7° sharp cone at zero angle of attack in two hypersonic tunnels under conventional and quiet noise levels.[13–16] Experiments under noisy flow were conducted in the Sandia National Laboratories Hypersonic Wind Tunnel (HWT) at Mach 5, 8, and 14. These measurements showed that the transitional boundary layer at high Mach numbers is complicated. There are large regions of second-mode instability waves intermixed with turbulence.[17] Traditional low speed intermittency computation methods only consider turbulent/non-turbulent regions.[8,9] However, for hypersonic flow, large regions of second-mode instability waves are observed in the transition region, along with turbulent regions. These waves include large surface pressure fluctuations which must be considered when developing appropriate models of the transitional pressure field.

The simultaneous surface pressure measurements and schlieren images from Ref. 17 are used in the present work to develop methods of distinguishing second-mode instability waves from turbulence. Separate

but complimentary methods are developed for both the surface pressure measurements as well as for the schlieren videos. These are used to compute the intermittency of both the instability waves and turbulent spots throughout transition over a range of M and Re.

II. Experimental Setup

II.A. Sandia Hypersonic Wind Tunnel

The Sandia Hypersonic Wind Tunnel (HWT) is a conventional blowdown-to-vacuum facility. Interchangeable nozzle and heater sections allow the tunnel to be run at Mach 5, 8 or 14. Run times were typically 30 s. Mach 5 tests use air as the driver gas. HWT-5 has a P_0 range of 345–1380 kPa and a T_0 range of 330–890 K, giving a Re range of 3.3–26 $\times 10^6/m$. Noise levels vary from 1–2% in this tunnel.[13] HWT-8 uses 689 MPa nitrogen supplied from a bottle farm. It has a P_0 range of 1720–6890 kPa, T_0 range of 500–890 K, and Re can be varied from 3.3–20 $\times 10^6/m$. Noise levels vary from 3–5%.[13]

Freestream conditions in this tunnel are computed using the Beattie-Bridgeman model to account for real-gas effects. At the low freestream temperatures in these tunnels, a linear viscosity law is used. Edge conditions used for normalization of the data were computed using a Taylor-Maccoll solution for flow over the cone.

II.B. High-Speed Schlieren System

A high-speed schlieren system was developed to take images at a high frequency while also being able to resolve the detailed structure of the boundary-layer disturbances. Fig. 2 shows a simple schematic of the final system design. Figs. 3(a) and 3(b) show pictures of the setup.

The light source was a Flashpoint II 1220A Monolight which emits white light. This light has a flash energy rating of 600 Watt-seconds and a flash duration between 1–2 ms. The light could be fired every 2.5 seconds, allowing ten short movies to be captured during a typical run. The light from the source was passed through a slit to increase sensitivity and provide a more well-defined effective source. Two 101.6-mm diameter convex lenses with a 1-m focal length were then used to collimate the remaining light, pass it through the test section, and focus the light on a knife edge. The lenses were equally spaced on either side of the tunnel centerline. Most of the light was cutoff at the knife edge in order to increase the sensitivity of the schlieren system. The remaining light was then passed to a Phantom v12.1 digital camera. The slit, knife edge, and camera were all tilted 7° from horizontal to line up with the cone surface.

The Phantom camera was used for its high light sensitivity, fast imaging capabilities, and short exposure time. The camera has a fill factor of 56% and a 20 μm pixel size. The minimum exposure time of 285 ns was used for all images. The lens used with the camera was varied between a 85, 105, and 180-mm lens with f-stops of f/1.8, f/2.8, and f/3.5, respectively. The 180-mm lens was typically used at Mach 5 to give better resolution in the thin boundary layer. The 105-mm lens was mostly used for Mach 8 and 14; resolution was sacrificed in order to retain more light needed at the lower freestream densities at higher M. The exact resolution and framing rate f was changed from run to run. Typical framing rates varied between 70–300 kHz. The array size varied between 1024×80 pixels and 512×32 pixels for these framing rates. Three to six hundred usable images were captured per movie; the exact number depended on the framing rate for a given run.

The schlieren images integrate through a curved boundary layer which will have some effect on the data. The maximum azimuthal integration length at the middle of the schlieren viewing area was estimated by calculating the length of the circular segment at the radius of the cone R plus the boundary layer thickness δ, at a height R. At Mach 5 at a Re of $4.39 \times 10^6/m$, the boundary layer thickness is approximately 1.3 mm as determined optically from the schlieren images. This gives a maximum azimuthal integration length of approximately 17 times the boundary-layer thickness. At Mach 8 at a similar Re, the maximum azimuthal integration length is approximately 12 δ (δ is approximately 2.4 mm).

Images were post-processed by applying a flat-field correction. The images were then contrast enhanced to emphasize the boundary-layer disturbances; the top 0.1% of the images was saturated. A gamma correction ($\gamma = 1.5$) was applied to nonlinearly weight the images towards darker values.

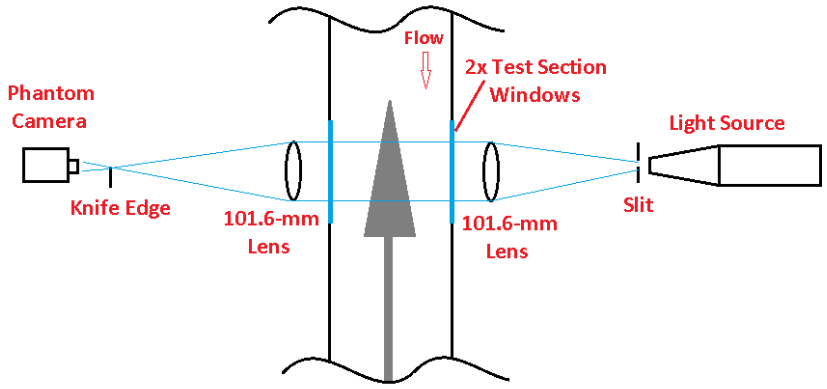

Figure 2. Schematic of the high-speed schlieren system developed for the Sandia Hypersonic Wind Tunnel.

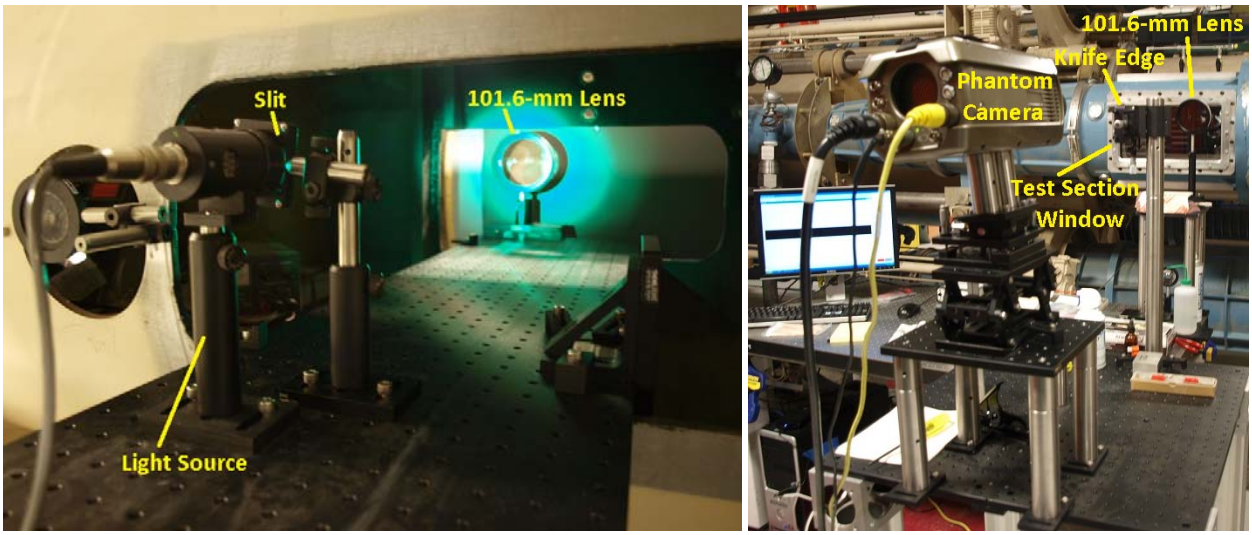

(a) (b)

Figure 3. High-speed schlieren system. The LED light source used for alignment is shown in place of the Flashpoint Monolight.

II.C. Model and Instrumentation

A 0.517-m-long 7° half-angle stainless-steel cone with a sharp nose (radius less than 0.05 mm) was used for this work (Fig. 4(a)). This cone has been used in previous experimental campaigns,[13–17] but the current analysis focuses on simultaneous schlieren and pressure measurements from Ref. 17. An axial array (Fig. 4(b)) with five PCB132 pressure sensors spaced 5.1 mm apart was used for pressure measurements. The fourth PCB132 sensor at x = 0.386 m was not working for these tests. There are additional Mic-062 Kulite pressure sensors in the axial array but those measurements are not discussed here. A downstream PCB132 pressure sensor was also located in a spanwise insert at x = 0.452 m. The schlieren viewing area was centered around the axial array (between x = 0.326 and 0.416 m) to allow simultaneous schlieren imaging and high-frequency pressure measurements. Table 1 list the location of the pressure sensors and the schlieren viewing area.

The growth and breakdown of the second-mode instability leading to transition can be studied with the PCB132 sensors. The sensor is a very high frequency piezoelectric time-of-arrival sensor. The resonant frequency is above 1 MHz; however, the sensor output is high-pass filtered at 11 kHz, per the manufacturer's specifications. Because the PCB132's can measure pressure fluctuations between 11 kHz and 1 MHz, they allow a study of instability breakdown to transition and are useful indicators of transition on the model.

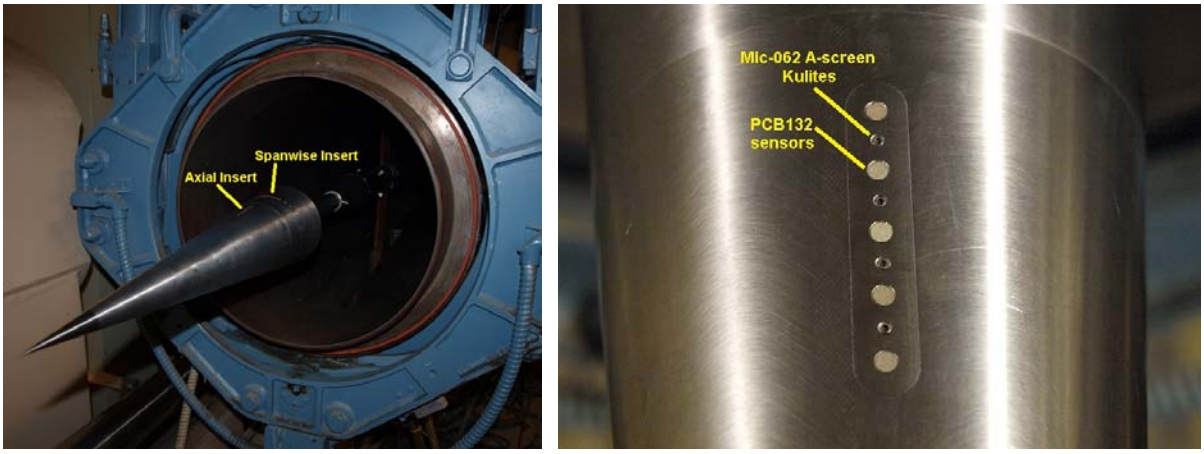

(a) (b)

Figure 4. Wind-tunnel model (a) Cone installed in Sandia Hypersonic Wind Tunnel; (b) Close-up view of axial insert showing closely spaced pressure instrumentation.

Table 1. Axial location of schlieren viewing area and pressure sensors on the 7° cone.

Location	Sensor	x (m)
Beginning of Schlieren Viewing Area		0.326
A1	PCB132	0.355
A3	PCB132	0.365
A5	PCB132	0.376
A7	PCB132	0.386
A9	PCB132	0.396
End of Schlieren Viewing Area		0.416
Spanwise Insert	PCB132	0.452

Also, the sensors have adequate frequency response to resolve the short duration of turbulent spots on the cone. However, the amplitude response of the sensors has not yet been accurately calibrated. In addition, the sensors have spatial resolution limitations. Second-mode waves have a wavelength of approximately twice the boundary-layer thickness (δ is about 1–3 mm for measurements on a typical cone model). The PCB132 diameter (3.18 mm) is larger than half of the instability wavelength on the cone. The actual sensitive area of the face is smaller, but its exact area is unknown. Some initial calibration work has been completed,[18,19] but more in-depth calibration is still needed. A shock tube has recently been built at Purdue for these purposes.[20]

II.D. Data Acquisition

The PCB132 sensors all run through a PCB 482A22 signal conditioner that provides constant-current excitation to the built-in sensor amplifier. It also decouples the AC signal from the DC bias voltage. The output from the signal conditioner is fed through a Krohn-Hite Model 3944 Filter with a 1.25 MHz low-pass anti-aliasing Bessel filter. This filter has four poles and offers 24 dB of attenuation per octave. The sampling frequency for the PCB132 sensors was 2.5 MHz. Pressure sensor data was acquired using a National Instruments PXI-1042 chassis with 14-bit PXI-6133 modules (10 MHz bandwidth). Ten 0.2-s segments of data were acquired every 2.5 seconds during each run. These segments were triggered by a Stanford Research Systems DG645 Digital Delay Generator that also simultaneously triggered the light source and camera of the schlieren system.

III. Experimental Results

Methods to separate instability waves from turbulence were developed for both the surface pressure measurements and simultaneous schlieren videos. Consider first a transitional case at Mach 5. Fig. 5 shows a typical schlieren sequence at an intermediate Re of $9.75 \times 10^6/m$. The red arrows mark the location of four PCB132 sensors beneath the viewing area at x = 0.355, 0.365, 0.376, and 0.396 m. In this case, a low-frequency disturbance is seen convecting within a smooth, laminar boundary layer (Figs. 5(a) – 5(b)). Higher frequency periodic waves develop on top of this low-frequency disturbance (Figs. 5(c) – 5(d)). The disturbance then breaks down into a turbulent spot that continues to convect and grow downstream (Figs. 5(e) – 5(g)). Stability analyses show that the low-frequency disturbance is likely a first-mode wave, while higher frequency periodic disturbances are second-mode instability waves.[17]

Fig. 6 shows simultaneous pressure traces and the corresponding power spectral densities (PSD's) for this case. The bounding times of the schlieren sequence are shown with vertical black lines. The traces are offset from each other proportional to their axial location on the cone in order to show the growth and convection of boundary-layer disturbances. PSD's were computed from these 200 μs pressure traces using a Blackman window. Because only a single time trace is used for the computation, the plots are noisy (there is no averaging). Also, because of the short time traces used, the resolution of the spectra is only 5 kHz. However, the spectra can still indicate the frequency of the boundary-layer disturbances.

The pressure trace from the first sensor at x = 0.355 m shows large high-frequency waves passing by, in agreement with the schlieren images. The corresponding PSD shows a peak between 200 and 400 kHz, at a range expected for the second-mode instability. The low-frequency first-mode disturbance is not observed in the surface pressure fluctuations, but may be obscured freestream tunnel noise which is largest at low frequencies. The pressure traces from the last three sensors between x = 0.365 and 0.396 m show a turbulent disturbance passing by, also in agreement with the schlieren images. The corresponding spectra indicate more broadband frequencies as expected for a turbulent disturbance.

It is desired to compute the transition statistics directly from the surface pressure measurements. A typical low-speed method to characterize boundary-layer intermittency is given by Ching and Lagraff.[21] This technique has been used previously to calculate boundary-layer intermittency in high-speed flow.[22] The method was able to distinguish disturbances from laminar flow, but could not separate instability waves from turbulence.

An improved method to identify the disturbances and also distinguish instabilities from turbulence was developed using the wavelet transform. This technique shows the frequency content of the disturbances as a function of time, and has been used in other unsteady applications such as wake transition, meteorological studies, and cavity flows.[23–25] The transform provides good time resolution for identifying intermittent

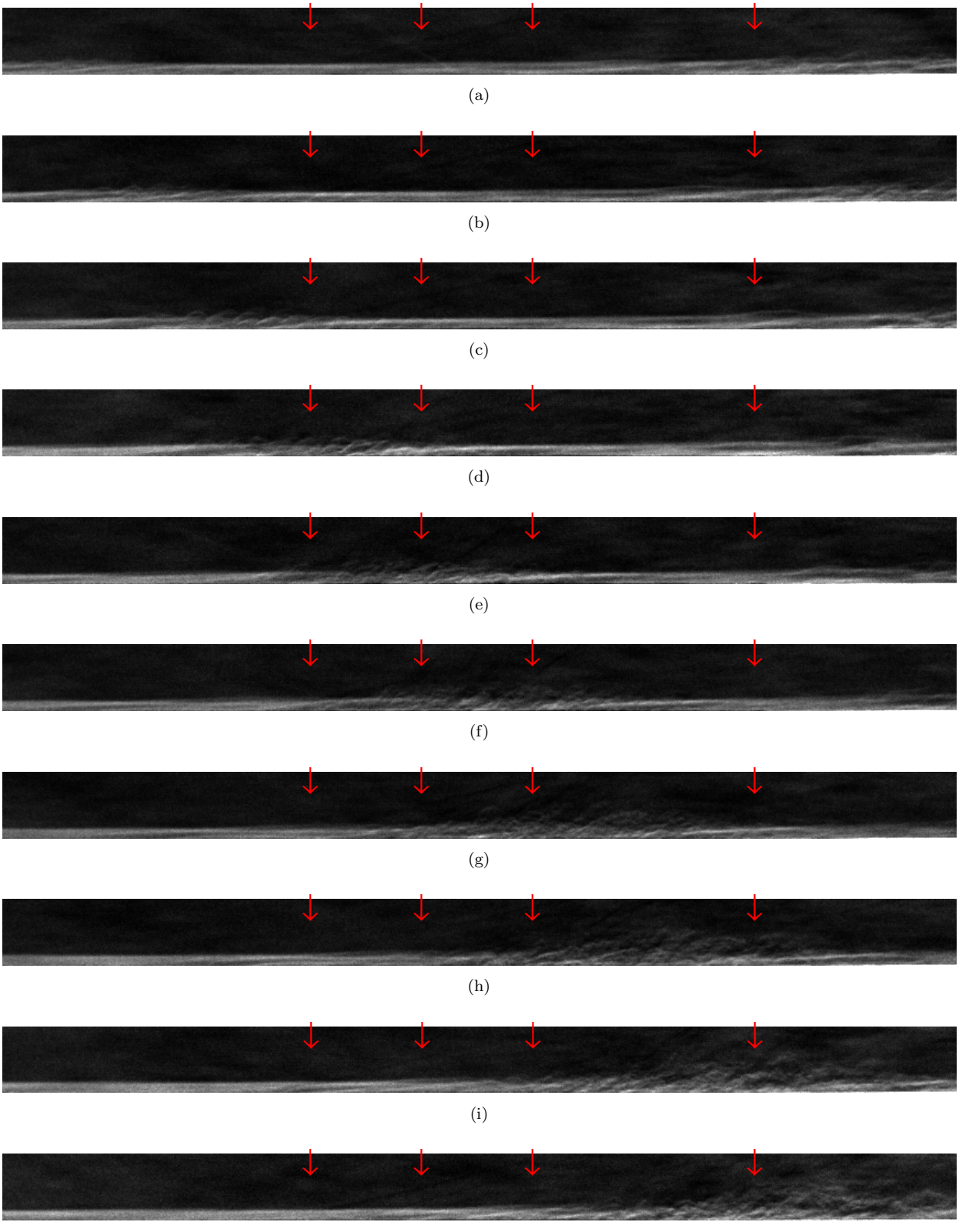

Figure 5. Schlieren images showing intermittent disturbances within mostly laminar flow, HWT-5, $t = 0.669 - 0.768\ ms$**,** $f = 91\ kHz$**,** 1024×64 **pixel array size,** $Re = 9.75 \times 10^6/m$**,** $M = 4.96$**,** $P_0 = 650.3\ kpa$**,** $T_0 = 446.6\ K$**.**

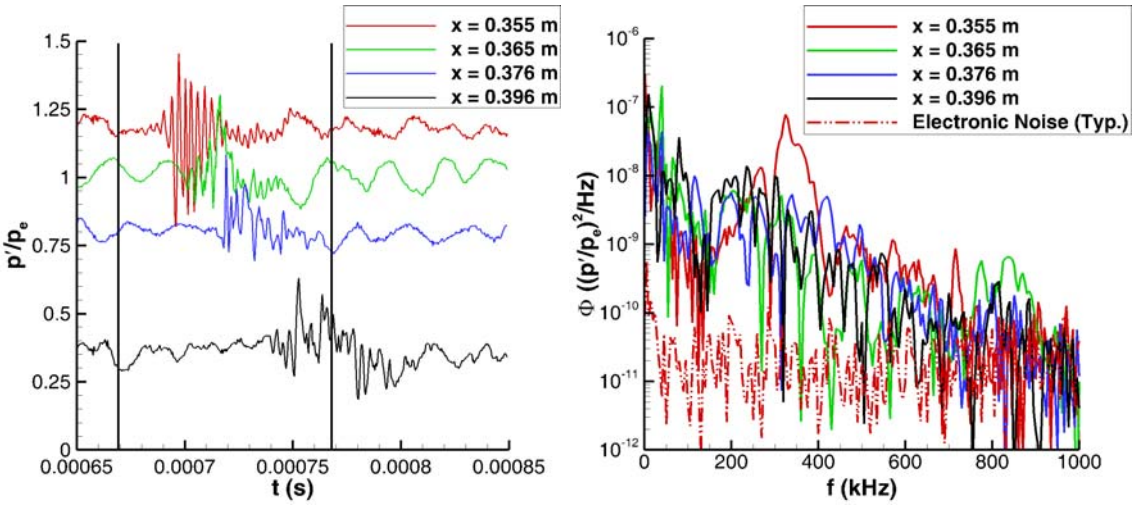

(a) (b)

Figure 6. Simultaneous pressure measurements, HWT-5, $Re = 9.75 \times 10^6/m$, $M = 4.96$, $P_0 = 650.3\ kpa$, $T_0 = 446.6\ K$ **(a) Pressure traces, each trace is vertically offset proportional to x. Vertical black lines mark the time of the corresponding schlieren images; (b) Power-spectral densities.**

disturbances. However, it has poor frequency resolution compared to alternate joint time-frequency methods such as the short-time-Fourier transform.

Fig. 7 shows an example of the wavelet transform computed for the pressure traces in Fig. 6(a) as well as for a downstream sensor at x = 0.452 m. The evolution of the frequency content of the disturbance can be clearly seen with downstream distance. At x = 0.355 m, the disturbance is still an instability wave packet. High levels of frequency content are concentrated between 200-600 kHz. Further downstream, the wave packet breaks down into a turbulent spot. High frequency content is still observed above 200 kHz, though at a reduced level. The region of high-frequency content also spreads in time as the disturbance grows and more turbulent regions develop in the flow. A low-frequency portion of the spectra also develops between 50–150 kHz and grows in amplitude with downstream distance.

A threshold criteria based on different frequency ranges in the transform can be used to separate the second-mode waves and turbulence. It is difficult to distinguish large, nonlinear second-mode waves from turbulence in the high-frequency range of the wavelet transform, since those high frequencies are common to both. Instead, the low frequency range between 50 and 150 kHz can be used to identify turbulent spots. A threshold criteria is first applied over that region to determine if the region is turbulent. If the region is not identified as turbulent, then a separate threshold criteria on the results between 200 and 400 kHz are used to identify regions of instability waves. This technique effectively uses the wavelet transform as a band-pass filter on the data.

The results of applying this two-step technique for this case are shown in Fig. 8. Elevated dotted lines identifying turbulent regions and dashed lines indicating areas of second-mode waves are shown superimposed on the pressure traces. This method is successfully able to distinguish the two disturbances. Periodic components corresponding to the instability waves are captured, while more turbulent regions are similarly identified. The method is also able to identify regions of waves at the leading and trailing edges of turbulent spots, as was often observed in Ref. 22.

An analogous procedure to distinguish second-mode waves from turbulence was developed for the schlieren images. A 'Canny' edge detection method was first used to find edges in the schlieren images. This method finds the local maxima of the gradient of the images. The gradient is calculated using the derivative of a Gaussian filter. A dual threshold is used to detect both strong and weak edges in the images, but weak edges are maintained only if they are connected to strong edges. This dual threshold helps to distinguish weak edges from background noise in the images. Fig. 9 shows typical images of second-mode waves and turbulent spots with and without edges marked in red by this algorithm. The maximum y location of the edges was then found at each horizontal position. Local averages of the maximum edge locations were computed across the image (the length of the average was two times the laminar δ). These averages were then compared to the laminar boundary layer height δ. Values larger than the laminar δ were marked as turbulent (equal to

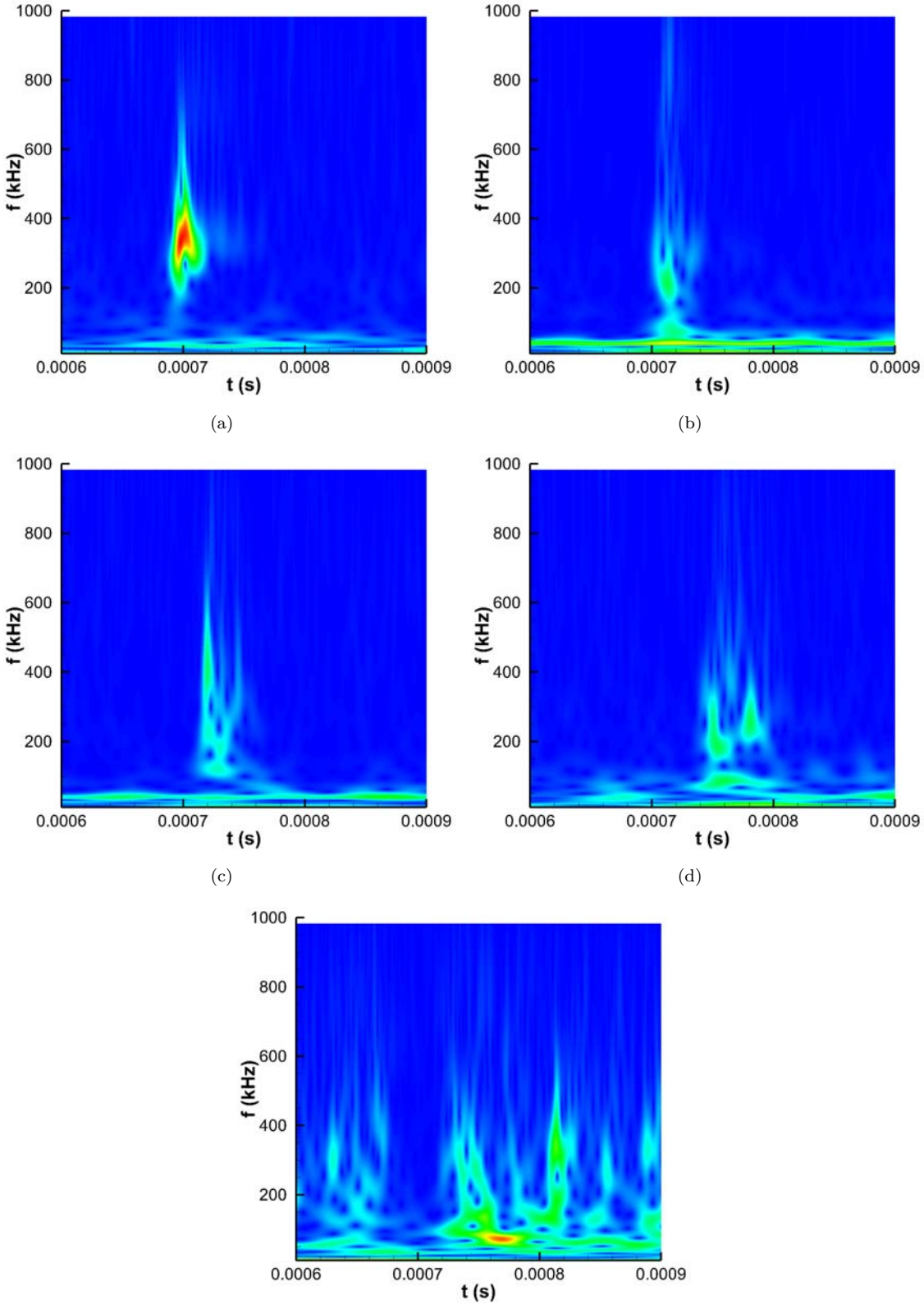

Figure 7. Wavelet transform of pressure measurements, HWT-5, $Re = 9.75 \times 10^6/m$ **(a) x = 0.355 m; (b) x = 0.365 m; (c) x = 0.376 m; (d) x = 0.396 m; (e) x = 0.452 m.**

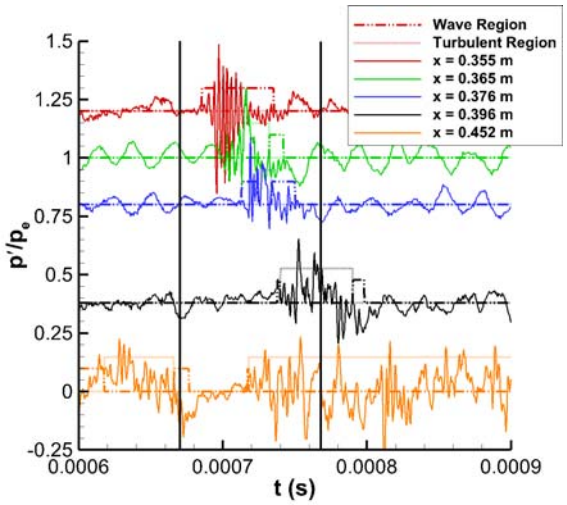

(a)

Figure 8. Wavelet transform thresholds applied to pressure measurements to distinguish turbulence and second-mode waves, HWT-5, $Re = 9.75 \times 10^6/m$**.**

1), while those equal or less than the boundary-layer height were marked as laminar (equal to 0).

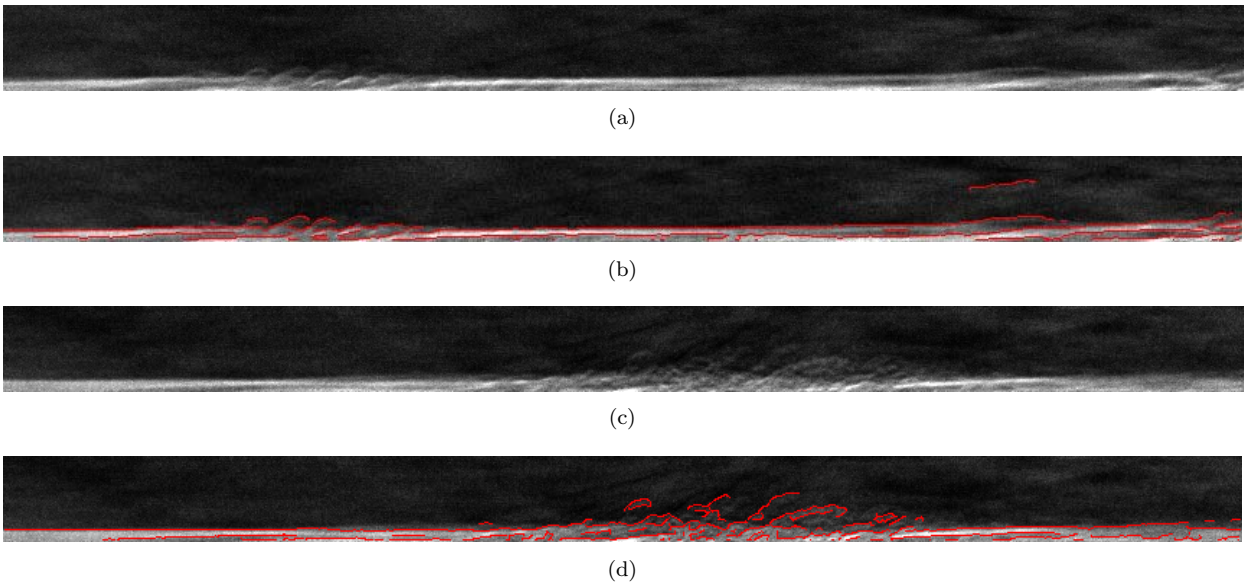

(a)

(b)

(c)

(d)

Figure 9. Edge detection in schlieren images, HWT-5, $Re = 9.75 \times 10^6/m$ **(a) Typical wave packet; (b) Packet with edges marked by the 'Canny' algorithm; (c) Typical turbulent spot; (d) Spot with edges marked by the 'Canny' algorithm.**

Second-mode waves are harder to distinguish in the schlieren images. A method based on the boundary-layer thickness does not work to pick out the waves, since the average boundary-layer height across regions of waves is near the laminar δ. Instead, an auto-correlation technique was used. Segments of the image (with a height of 1.5 and a length of 2 times the laminar δ, respectively) were auto-correlated within a longer region to identify any periodic components. Peaks in the autocorrelation at the expected second-mode wave frequency range were identified as instability waves.

This technique was applied to all images obtained during a schlieren video and the results were averaged to obtain intermittency curves along the schlieren viewing area. Intermittency results at this Re from both the pressure measurements and simultaneous schlieren images are shown in Fig. 10. There is reasonable agreement between the two techniques, though overall the schlieren images are not as sensitive to the second-mode waves as the pressure measurements. In this case, the intermittency of the second mode waves is near

0.2 and fairly constant if slightly decreasing with downstream distance. The turbulent intermittency is increasing from near zero to over 0.8 with downstream distance. The overall disturbance intermittency (sum of the instability and turbulent intermittencies) is also increasing with downstream distance, but does not reach one in this case. Because the intermittency of the instability waves remains low, there is not a large difference between the turbulent intermittency and the overall disturbance intermittency.

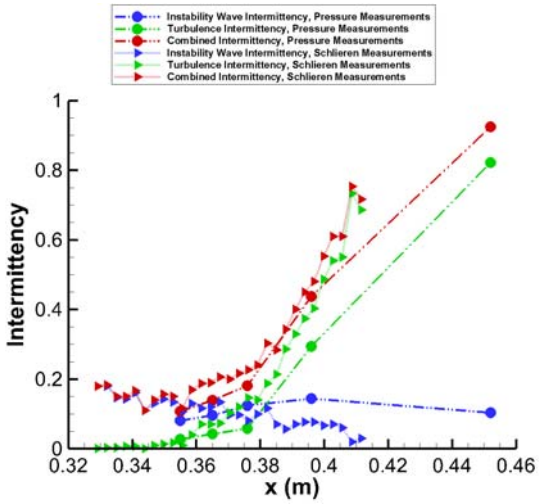

Figure 10. Intermittency along cone computed using the wavelet transform and schlieren techniques, HWT-5, $Re = 9.75 \times 10^6/m$.

Results at a higher Re of $11.8 \times 10^6/m$ are shown in Fig. 11(a). Transition begins further upstream in this case, though the overall trends are similar. The wave packet intermittency again begins near 0.2 but then decreases towards zero as the turbulent intermittency increases from zero to near one. The overall disturbance intermittency is high in this cases and approaches one. At the highest Re of $15.4 \times 10^6/m$ (Fig. 11(b)), the boundary layer is mostly turbulent. Some regions of second-mode waves are observed at the beginning of the schlieren viewing area, but the number of waves quickly decreases as fully turbulent flow is reached downstream. Again, the turbulent intermittency and overall disturbance intermittency are similar because the intermittency of second-mode instability waves remains small. This transitional behavior is similar to low-speed results since isolated disturbances are observed surrounded by an otherwise smooth, laminar boundary layer.

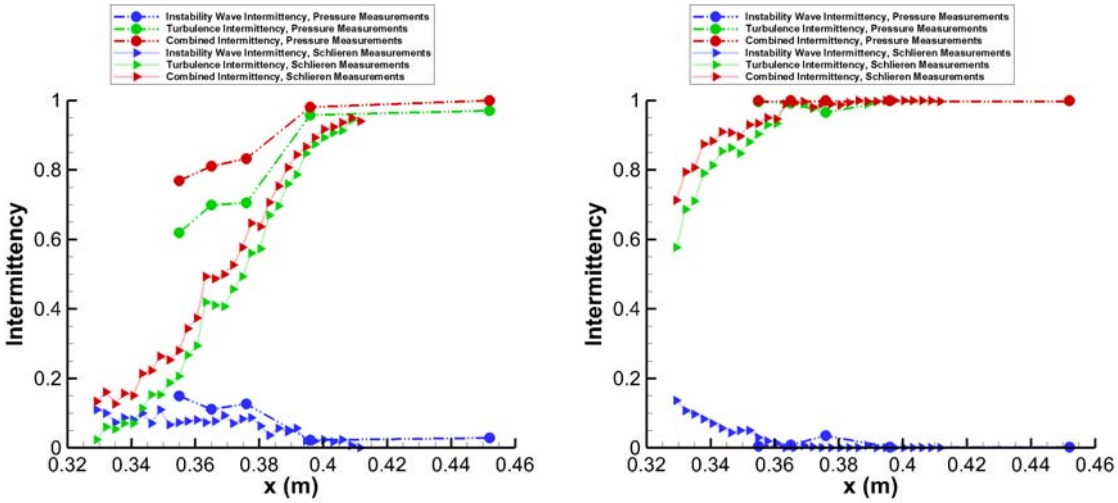

Figure 11. As Fig. 10, but (a) $Re = 11.8 \times 10^6/m$**; (b)**$Re = 15.4 \times 10^6/m$.

The same techniques were also applied to Mach 8 data. At this higher Mach number, the character of the boundary layer is different. Second-mode waves are prevalent throughout the viewing area, even before turbulent regions begin to appear.[17] A typical schlieren sequence is shown in Fig. 12 at a mid Re

of 7.08 $\times$ $10^6/m$. A patch of distorted waves is observed at the left of Fig. 12(a). This patch convects and grows downstream in subsequent images and appears to become turbulent by Fig. 12(e). Behind this patch, second-mode waves are again observed. At higher Re, more turbulent regions appear, intermixed with second-mode waves.[17]

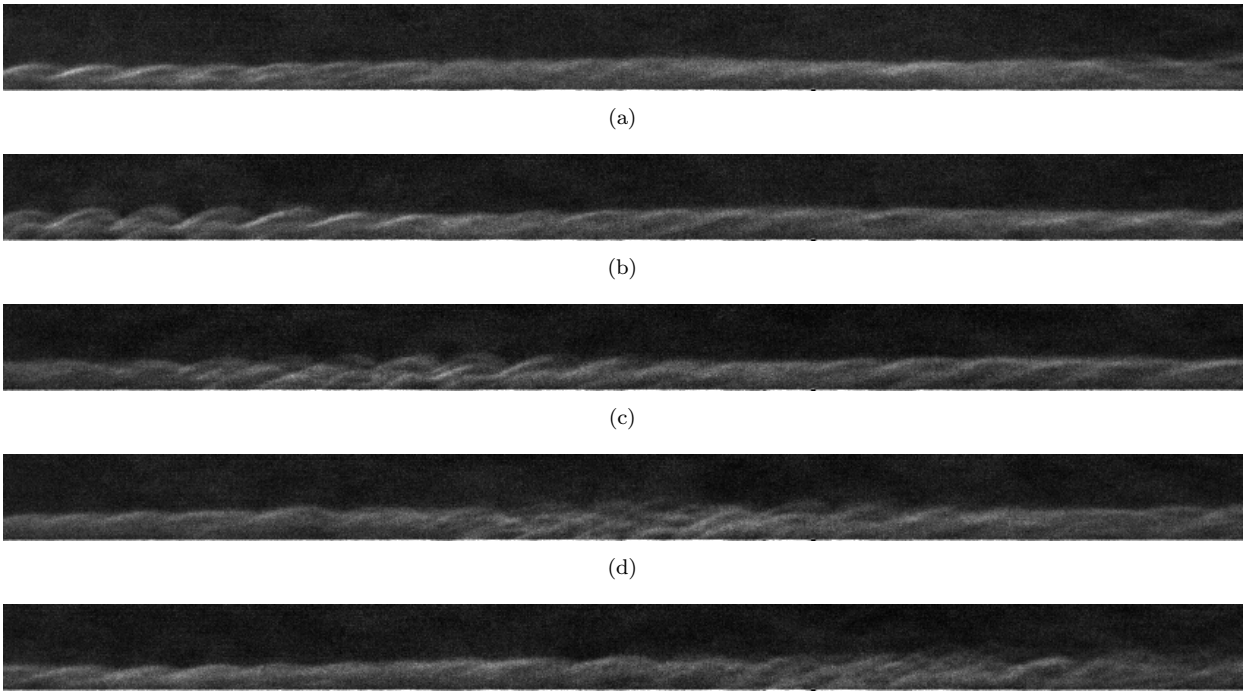

Figure 12. Schlieren images showing intermittent development of a turbulent spot within mostly second-mode waves, HWT-8, $t = 1.262 - 1.361\ ms$, $f = 91\ kHz$, 1024×64 **pixel array size,** $Re = 7.08 \times 10^6/m$, $M = 7.84$, $P_0 = 2429\ kPa$, $T_0 = 610\ K$.

This different boundary-layer character is captured by the intermittency results (Fig. 13(a)). As opposed to Mach 5, the intermittency of the second-mode waves reaches near one before turbulent spots appear. This is especially clear in the pressure measurements, which are more sensitive to small second-mode waves. Once turbulent spots appear, the intermittency of the wave packets decreases; however, the combined intermittency of the disturbances remains near one. A similar behavior is also seen at a higher Re of $9.7 \times 10^6/m$ (Fig. 13(b)). The overall disturbance intermittency remains near one through the transitional region; however, the instability intermittency is actually decreasing towards zero as the turbulence intermittency is increasing towards one.

At Mach 8, the overall disturbance and turbulent intermittencies are quite different throughout the transition region. This highlights the changing character of the boundary layer at high M. The prevalence of the instability waves is an added consideration when modeling the transitional boundary layer. If this intermittent character of the instability waves and turbulent spots can be incorporated into models at high M, then the transitional pressure fluctuations should be able to be more accurately captured than by using a method that only captures turbulent/non-turbulent regions.

IV. Concluding Remarks

Simultaneous high-frequency pressure and schlieren measurements were made of boundary-layer disturbances on a 7° cone in the Sandia Hypersonic Wind Tunnel over a range of M and Re. These measurements allowed the intermittent behavior of the boundary layer to be studied and highlighted how the transitional character of the boundary layer changes at higher Mach number from regions of isolated disturbances to a transitional region dominated by instability waves that then break down to turbulence.

The present work focused on distinguishing the instability waves from turbulent spots and determining the intermittency of each. A wavelet analysis technique was developed to separate instability waves from

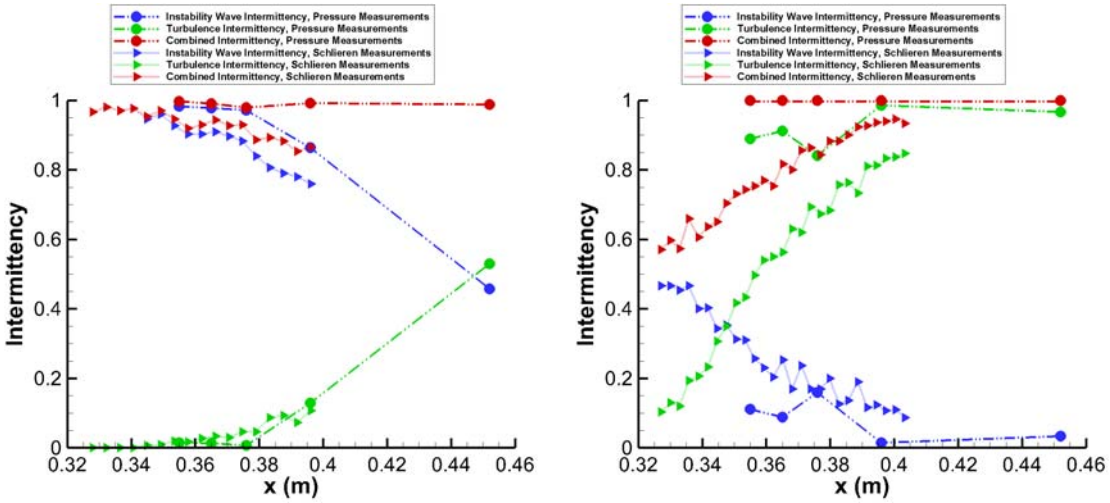

Figure 13. Intermittency curves computed using the wavelet transform and schlieren techniques, HWT-8 (a) $Re = 7.1 \times 10^6/m$**; (b)** $Re = 9.7 \times 10^6/m$**.**

turbulence in the pressure measurements. A different procedure was created for the schlieren measurements using a boundary-layer thickness criteria to mark turbulent regions and an auto-correlation technique to identify instability waves.

The intermittency results were similar between the two techniques and showed how the character of the boundary layer changed through transition. At a Mach number of 5, intermittent second-mode waves developed but were still isolated and remained at a low intermittency near 0.2. As the Mach number was increased to 8, second-mode instability waves became a more important part of transition. The intermittency of these waves was near one before regions of the instabilities began to break down to turbulence. The turbulent intermittency then rose as the instability intermittency fell. However, the overall disturbance intermittency remained near one throughout this transitional region.

These techniques will next be used to calculate additional statistics of these individual disturbances, including the burst rate and distribution of burst length along the cone. By combining this statistical information about the disturbance formation with the pressure structure and growth properties of the disturbances, the pressure fluctuations at a given location on the cone should be able to be computed using a turbulent-spot model of the transition process. This will provide a data set for developing predictive models of a flight vehicle's environment.

Acknowledgments

Wavelet software was provided by C. Torrence and G. Compo, and is available at URL: http://paos.colorado.edu/research/wavelets/.[24]

References

[1]Laganelli, A. L., Martellucci, A., and Shaw, L. L., "Wall Pressure Fluctuations in Attached Boundary-Layer Flow," *AIAA Journal*, Vol. 21, No. 4, 1983, pp. 495–502.

[2]Pate, S. R. and Brown, M. D., "Acoustic Measurements in Supersonic Transitional Boundary Layers," AEDC-TR-69-182, October 1969.

[3]Johnson, R. I., Macourek, M. N., and Saunders, H., "Boundary Layer Acoustic Measurements in Transitional and Turbulent Flow at $M_\infty = 4.0$," AIAA Paper 69-344, April 1969.

[4]Cassanto, J. M. and Rogers, D. A., "An Experiment to Determine Nose Tip Transition with Fluctuating Pressure Measurements," *AIAA Journal*, Vol. 13, No. 10, October 1975, pp. 1257–1258.

[5]Martellucci, A., Chaump, L., Rogers, D., and Smith, D., "Experimental Determination of the Aeroacoustic Environment about a Slender Cone," *AIAA Journal*, Vol. 11, No. 5, 1973, pp. 635–642.

[6]Pate, S. R., "Dominance of Radiated Aerodynamic Noise on Boundary-Layer Transition in Supersonic/Hypersonic Wind Tunnels," AEDC-TR-77-107, March 1978.

[7]Johnson, C. B., Stainback, P. C., Wicker, K. C., and Boney, L. R., "Boundary-Layer Edge Conditions and Transition Reynolds Number Data for a Flight Test at Mach 20 (Reentry F)," NASA TM X-2584, July 1972.

[8]Dhawan, S. and Narasimha, R., "Some Properties of Boundary Layer Flow During the Transition from Laminar to Turbulent Motion," *Journal of Fluid Mechanics*, Vol. 3, No. 4, 1958, pp. 418–435.

[9]Narasimha, R., "The Laminar-Turbulent Transition Zone in the Boundary Layer," *Progress in Aerospace Sciences*, Vol. 22, January 1985, pp. 29–80.

[10]Vinod, N., "The Signature of Laminar Instabilities in the Zone of Transition to Turbulence," *Journal of Turbulence*, Vol. 8, No. 2, 2007.

[11]Zharov, V. A., Htun, H., and Khlopkov, Y. I., "Statistical Modeling of the Turbulent Transition in the Boundary Layer," *Journal of Applied Mechanics and Technical Physics*, Vol. 50, No. 5, 2009, pp. 742–746.

[12]Park, S. and Lauchle, G., "Wall Pressure Fluctuation Spectra Due to Boundary-Layer Transition," *Journal of Sound and Vibration*, Vol. 319, 2009, pp. 1067–1082.

[13]Casper, K. M., *Hypersonic Wind-Tunnel Measurements of Boundary-Layer Pressure Fluctuations*, Master's Thesis, Purdue University, School of Aeronautics & Astronautics, August 2009.

[14]Casper, K. M., Beresh, S. J., Henfling, J. F., Spillers, R. W., Pruett, B. O. M., and Schneider, S. P., "Hypersonic Wind-Tunnel Measurements of Boundary-Layer Pressure Fluctuations," AIAA Paper 2009-4054, June 2009.

[15]Alba, C. R., Casper, K. M., Beresh, S. J., and Schneider, S. P., "Comparison of Experimentally Measured and Computed Second-Mode Disturbances in Hypersonic Boundary-Layers," AIAA Paper 2010-897, January 2010.

[16]Casper, K. M., Beresh, S. J., Henfling, J. F., Spillers, R. W., and Pruett, B. O. M., "High-Speed Schlieren Imaging of Disturbances in a Transitional Hypersonic Boundary Layer," AIAA Paper 2013-0376, January 2013.

[17]Casper, K. M., Beresh, S. J., Wagnild, R. M., Henfling, J. F., and Spillers, R. W., "Simultaneous Pressure Measurements and Schlieren Imaging of Disturbances in a Hypersonic Boundary Layer," AIAA paper to appear, June 2013.

[18]Beresh, S. J., Henfling, J. F., Spillers, R. W., and Pruett, B. O. M., "Fluctuating Wall Pressures Measured beneath a Supersonic Turbulent Boundary Layer," *Physics of Fluids*, Vol. 23, 075110, 2011.

[19]Berridge, D. C., *Measurements of Second-Mode Instability Waves in Hypersonic Boundary Layers with a High-Frequency Pressure Transducer*, Master's Thesis, Purdue University School of Aeronautics & Astronautics, December 2010.

[20]Ward, C. A. C., Wheaton, B. M., Chou, A., Berridge, D. C., Letterman, L. E., Luersen, R. P. K., and Schneider, S. P., "Hypersonic Boundary-Layer Transition Experiments in the Boeing/AFOSR Mach-6 Quiet Tunnel," AIAA Paper 2012-0282, January 2012.

[21]Ching, C. Y. and LaGraff, J. E., "Measurements of Turbulent Spot Convection Rates in a Transitional Boundary Layer," *Experimental Thermal and Fluid Science*, Vol. 11, 1995, pp. 52–60.

[22]Casper, K., *Pressure Fluctuations Beneath Turbulent Spots and Instability Wave Packets in a Hypersonic Boundary Layer*, Ph.D. Thesis, Purdue University School of Aeronautics & Astronautics, August 2012.

[23]Jordan, D., Miksad, R. W., and Powers, E. J., "Implementation of the Continuous Wavelet Transform for Digital Time Series Analysis," *Review of Scientific Instruments*, Vol. 68, No. 3, March 1997, pp. 1484–1494.

[24]Torrence, C. and Compo, G. P., "A Practical Guide to Wavelet Analysis," *Bulletin of the American Meteorological Society*, Vol. 79, No. 1, 1998, pp. 61–78.

[25]Kegerise, M.A. amd Spina, E. F., Garg, S., and Cattafesta, L. N., "Mode-Switching and Nonlinear Effects in Compressible Flow Over a Cavity," *Physics of Fluids*, Vol. 16, No. 3, March 2004, pp. 678–687.